Conjunctive Use of Tension Infiltrometry and Time-Domain Reflectometry for Inverse Estimation of Soil Hydraulic Properties

R. C. Schwartz* and S. R. Evett

ABSTRACT

Infiltration from a tension disc infiltrometer can be applied conjointly with time-domain reflectometry (TDR) measurements of soil water content to improve estimates of field hydraulic parameters. However, interpretation of TDR-measured water contents for use in inverse optimizations may be problematic when rods are partially within the wetted zone. The objective of this study was to assess if TDR-measured soil water contents in addition to cumulative infiltration could improve parameter estimability for the inverse optimization problem. Infiltration experiments were conducted with a 0.58-m-diam. cylinder packed with a loamy sand. Three trifilar TDR probes were inserted diagonally into the soil to measure transient water contents during infiltration. Inverse optimizations utilized cumulative infiltration, water contents from diagonally placed TDR probes, and a branch of the wetting water characteristic $\theta(h)$ from extracted soil cores. Measured $\theta(h)$ at one or more pressure heads was required in optimizations to provide a satisfactory description of the water characteristic in the dry region. Optimizations for three infiltration experiments yielded similar parameter estimates with overlapping 95% confidence intervals. The use of diagonal TDR-measured water contents improved the predicted redistribution of soil water and decreased covariances between parameter pairs that led to better parameter estimability. Optimized simulations predicted water contents in a three-dimensional region within 0.03 $m^3\ m^{-3}$ of values measured by buried horizontal TDR probes. Parameter estimates were relatively insensitive to changes in the assumed averaging depth transverse to TDR rods. For the diagonally placed probes, the dominant gradients in water content were in directions that minimized errors associated with assuming a uniform weighting of water content within the TDR sampling volume.

Inverse optimization of parameters offers an efficient means to infer soil hydraulic properties from tension disc infiltrometer data. Šimůnek and van Genuchten (1996, 1997) concluded that identifiability of parameters was improved when optimizations included measured water contents or pressure heads as well as cumulative infiltration. Use of TDR to measure water contents during infiltration probably has the greatest potential for field applications because the response time of the instrument is fast, measurements are valid for essentially all water contents, and the rigidity and small diameter of probes permit their insertion into the soil with little resulting disturbance to the flow field. However, TDR measurements average soil water content in a sample volume with spatially distributed sensitivities. Inverse parameter optimization with TDR data therefore requires the integration of water contents simulated by Richards' equation across an *effective* soil volume. Moreover, the presence of a wetting front can influence the spatial sensitivity of TDR probes and bias the estimates of optimized parameters (Ferré et al., 2002).

Several studies have measured transient soil water contents using TDR during three-dimensional axial-symmetric flow. Kachanoski et al. (1990) used both curved- and straight-wave guides to monitor the wetting front progression and estimate cumulative infiltration from a point source. Wang et al. (1998) used horizontally buried probes to measure soil water contents during infiltration and estimate soil hydraulic parameters based on quasianalytical solutions. Because probes were buried, this precludes the use of these methodologies in field applications where an undisturbed soil condition is desired. Schwartz and Evett (2002) used TDR in conjunction with cumulative infiltration to inversely optimize hydraulic parameters for a fine-textured soil in the field. Probes were inserted diagonally at 45° from the soil surface to minimize soil disturbance. They obtained good agreement between measured and predicted water contents at late times when the wetting front had extended deeper into the profile. However, measured TDR water contents were significantly underestimated by the optimized solution at early times. They attributed the poor estimation of TDR water contents at early times to physical nonequilibrium processes during transient flow near the margins of the wetting front. The assumption of uniform weighting of water content (and the dielectric constant) across the three-dimensional sampling volume of the trifilar probes in the presence of the wetting front (Knight et al., 1994; Ferré et al., 1998) may also have biased calculated water contents.

In the present study, we attempted to minimize nonequilibrium flow by using a column of repacked soil. We compared water contents measured by diagonally placed TDR probes with predicted water contents obtained from inverse optimization of hydraulic parameters. We also examined the predicted patterns of wetting around the TDR probes to evaluate the degree to which TDR readings were influenced by nonuniform weighting of measured dielectric permittivity. Our objective was to evaluate the usefulness of ancillary soil water content data obtained by TDR and soil water characteristic data obtained from extracted soil cores for inverse estimation of soil hydraulic parameters.

MATERIALS AND METHODS

Infiltration experiments were completed with a 0.58-m-diam. cylinder packed with Vingo loamy fine sand (coarse-loamy, mixed, superactive, mesic Aridic Paleustalf) obtained from the 0- to 0.3-m soil depth. Soil with a volumetric water content of 0.07 $m^3\ m^{-3}$ was incrementally packed into the cylinder to a bulk density of 1.61 Mg m^{-3} (SD = 0.02) and to

Conservation and Production Research Laboratory, USDA-ARS, P.O. Drawer 10, Bushland, TX 79012-0010. Received 13 Mar. 2003. Special Section—Advances in Measurement and Monitoring Methods. *Corresponding author (rschwart@cprl.ars.usda.gov).

Published in Vadose Zone Journal 2:530–538 (2003).

677 S. Segoe Rd., Madison, WI 53711 USA

Abbreviations: TDR, time-domain reflectometry; VGM, van Genuchten-Mualem.

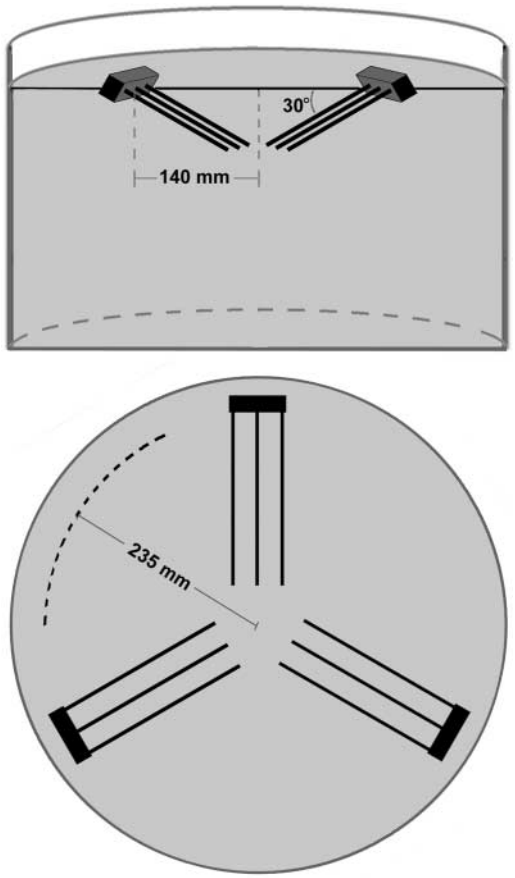

Fig. 1. Diagonally placed time-domain reflectometry (TDR) probes shown in a vertical cross section of the cylinder (above) and horizontally placed TDR probes shown in a horizontal cross section (below).

a depth of 0.40 m. At soil depths of 50, 100, 150, and 200 mm, three trifilar 0.2-m probes were installed horizontally as the soil was packed (Fig. 1). Additionally, three 0.15-m trifilar probes were inserted at a 30° angle into the soil surface, 40 mm from the disc infiltrometer's edge, and oriented toward the vertical axis of the infiltrometer (Fig. 1). Once the soil was packed and all probes were positioned, the cylinder was saturated from the bottom with 0.001 *M* $CaSO_4$. Thereafter, suction was applied at the bottom to drain the soil to an average water content of 0.12 ± 0.02 $m^3\ m^{-3}$ as determined with the horizontally positioned TDR probes at all depths.

A 0.2-m-diam. disc infiltrometer filled with 0.001 *M* $CaSO_4$ was used to measure cumulative infiltration at a nominal supply pressure head of $h_0 = -155$ mm H_2O. Before each infiltration run, the soil surface was leveled and a small amount (~1 mm depth) of Vingo soil passing a 0.5-mm sieve was sprinkled uniformly across the surface to facilitate contact between the soil surface and the nylon membrane of the infiltrometer. Water level in the infiltrometer reservoir tube was monitored with a pressure transducer at no more than 7.5-s intervals. Water contents were measured every 180 s using a TDR cable tester (Tektronic, Inc., Beaverton, OR, model 1502C)[1] connected to TDR probes through a coaxial multiplexer (Dynamax, Inc., Houston, TX, model TR-2001) (Evett, 1998), both of which were controlled by a laptop computer running the TACQ program (Evett, 2000a, 2000b). The trifilar probes had rod diameters of 3.2 mm and an outer rod separation distance of 60 mm. We used the polynomial function of Topp et al. (1980) to estimate water content from measurements of apparent permittivity. Three infiltration experiments were completed for this study. Supply pressure was maintained at a constant head of −155 mm for Exp. 1 and 2, whereas a series of ascending h_0's were imposed during Exp. 3 (Table 1). After each infiltration run, suction was applied at the bottom to facilitate drainage. Following drainage, soil water contents were permitted to equilibrate for at least a week before initiating another infiltration run.

[1] The mention of trade or manufacturer names is made for information only and does not imply an endorsement, recommendation, or exclusion by the USDA-ARS.

Table 1. Summary of disc-infiltrometer experiments.

Run	$\theta(z_1)$†	h_0‡	Duration
	$m^3\ m^{-3}$	mm H_2O	h
1	0.128	−155	1.0
2	0.115	−155	1.0
3§	0.117	−160, −102, −51, −2	1.0, 0.5, 0.33, 0.25

† Initial water content at the 50-mm soil depth (average of three time-domain reflectometry measurements).
‡ h_0, supply pressure head.
§ An ascending series of step-changes in h_0 were applied in Run 3.

Upon termination of all infiltration experiments, 13 soil cores (30-mm length × 54-mm diam.) were extracted from the cylinder at the depth increment of 10 to 40 mm. The soil cores were placed on a pressure plate apparatus at 100 kPa and permitted to equilibrate to an average water content of 0.082 (SD = 0.015) $m^3\ m^{-3}$. Subsequently, wetting water characteristic curves were obtained using a glass bead tension table with hanging water column at suctions ranging from 0.62 to 0.06 kPa.

Radially symmetric, two-dimensional water flow was described with the following form of Richards' equation (Warrick, 1992):

$$\frac{\partial\theta}{\partial t} = \frac{\partial}{\partial z}\left[K(\theta)\left(\frac{\partial h(\theta)}{\partial z} - 1\right)\right] + \frac{1}{r}\frac{\partial}{\partial r}\left(r\ K(\theta)\frac{\partial h(\theta)}{\partial r}\right) \quad [1]$$

where θ is the volumetric water content ($m^3\ m^{-3}$), t is time (s), z is the vertical coordinate taken positive downwards (cm), K is hydraulic conductivity (cm s^{-1}), h is pressure head (cm), and r is the radial coordinate (cm).

The van Genuchten-Mualem (VGM) model (van Genuchten, 1980; van Genuchten and Nielsen, 1985)

$$\theta(h) = \theta_r + \frac{\theta_s - \theta_r}{(1 + |\alpha h|^n)^m}$$
$$K(h) = K_s S^\tau [I_\zeta(p,q)]^2 \quad [2]$$

was used to describe the constitutive soil hydraulic properties of Eq. [1]. Here, θ_r and θ_s are the residual and saturated water contents ($m^3\ m^{-3}$), respectively, K_s is the saturated hydraulic conductivity (cm s^{-1}), S is the fluid saturation ratio $[\theta(h) - \theta_r]/(\theta_s - \theta_r)$, I_ζ is the incomplete beta function integrated from 0 to $\zeta = S^{1/m}$, $p = m + 1/n$, $q = 1 - 1/n$, and n, m, τ, and α (cm^{-1}) are empirically fitted parameters. Constraining $m = 1 - 1/n$ in the conductivity function of Eq. [2] yields the closed form solution of van Genuchten (1980)

$$K(h) = K_s S^\tau [1 - (1 - S^{1/m})^m]^2 \quad [3]$$

At pressure heads near saturation, $K(h)$ was also described by a piecewise loglinear interpolation (Schwartz and Evett, 2002)

$$K(h) = \begin{cases} \exp(L_0 \ln[K(h_{p0})] + L_1 \ln[K(h_{p1})]) & h_{p0} < h \le h_{p1} \\ \exp(L_1 \ln[K(h_{p1})] + L_2 \ln[K(h_{p2})]) & h_{p1} < h \le h_{p2} \\ \exp(L_2 \ln[K(h_{p2})] + L_3 \ln[K(h_{p3})]) & h_{p2} < h \le h_{p3} \end{cases} \quad [4]$$

where L_0, L_1, L_2, and L_3 are the Lagrangian coefficients for linear interpolation and h_{p0}, h_{p1}, h_{p2}, and h_{p3} are monotonically increasing pressure heads (cm).

Richards' equation was solved with a second-order, finite difference numerical method of lines procedure with variable step-size, variable order integration through time (Schwartz and Evett, 2002). A uniform, radial node spacing and a vertical node spacing increasing algebraically with depth was used for the finite difference grid. Solution tolerances and grid fineness were selected to ensure a mass balance error of <0.5% within the solution domain at all observed times throughout the infiltration experiments.

Inverse optimizations were completed with the procedures outlined by Schwartz and Evett (2002) and with the *IDSfit* code (Schwartz, 2002). The weighted objective function Φ (Eq. [9] of Schwartz and Evett, 2002) included the vectors of (i) cumulative infiltration depth through the infiltrometer base $\mathbf{I}(t,h_0)$, (ii) transient mean water contents measured by the diagonally placed (30°) TDR probes $\boldsymbol{\theta}_{TDR}(t)$, and (iii) measured water contents representing a portion of a wetting branch of the soil water characteristic curve $\boldsymbol{\theta}_{WC}(h)$. Four types of optimizations were performed under this study: (a) optimizations that used all of the measured data $\Phi(\mathbf{I},\boldsymbol{\theta}_{TDR},\boldsymbol{\theta}_{WC})$; (b) optimizations using only infiltration and the water characteristic $\Phi(\mathbf{I},\boldsymbol{\theta}_{WC})$; (c) optimizations using only infiltration and TDR-measured water contents $\Phi(\mathbf{I},\boldsymbol{\theta}_{TDR})$; and (d) optimizations of infiltration, TDR-measured water contents, and only one observation at h_1 of the water characteristic $\Phi[\mathbf{I},\boldsymbol{\theta}_{TDR},\boldsymbol{\theta}_{WC}(h_1)]$. Measured transient (TDR) and characteristic water contents were weighted 30 times greater than cumulative infiltration depth for all optimizations. This weighting factor was based on the variance of water contents measured by the diagonally placed TDR probes and an estimated variance for cumulative infiltration depth. Although the variances of water contents for the wetting characteristic curve were smaller than the variances of TDR data, these measurements were weighted equally because of the greater uncertainty associated with data obtained from extracted soil cores disconnected from the infiltration experiment. Trifilar TDR probes were assumed to sample water content in a volume defined by the rod length and a 80- × 30-mm plane transverse to the metallic rods. This region corresponds to approximately 90% of the sample area for trifilar probes with similar geometries (Ferré et al., 1998). The initial water content profile was estimated by a linear volume interpolation of soil water contents (Schwartz, 2002) measured by the buried, horizontal TDR probes.

RESULTS AND DISCUSSION

Optimizations with TDR-Measured Water Contents

Optimization results obtained by including the measured water characteristic in the objective function in addition to cumulative infiltration and TDR-measured water contents (Table 2) yielded close fits to all measured data for the first hour of cumulative infiltration (Fig. 2, 3). Fitted cumulative infiltration and TDR water contents for optimizations 1a and 2a (not shown) portray essentially identical patterns relative to measured values as that illustrated in Fig. 3 for the first hour of optimization 3a. For optimizations 1a, 2a, and 3.1a, m was set equivalent to $1 - (1/n)$ and τ was fixed at -0.50 to approximately satisfy the slope of $K(h)$ between -102 and -160 mm estimated with Wooding's solution (Schwartz and Evett, 2002) and also $\theta(h)$. Because opti-

Table 2. Results of inverse optimizations (a) with time-domain reflectometry (TDR) data included in the objective function and (b) without TDR data included in the objective function.

Opt†	Run	Time period	Weighted MSR‡			Parameter values§								
		h	I(t,h_0)	$\theta_{TDR}(t)$	$\theta_{WC}(h)$	θ_s	m	n	α	K_s	τ	$K(h_{p1})$	$K(h_{p2})$	$K(h_{p3})$
			¶			$m^3\ m^{-3}$			cm^{-1}	$cm\ s^{-1} \times 10^{-3}$		$cm\ s^{-1} \times 10^{-3}$		
			$\times 10^{-3}$			(a) Objective function of the type $\Phi(\mathbf{I},\boldsymbol{\theta}_{TDR},\boldsymbol{\theta}_{WC})$								
1a	1	0–1	3.049	1.208	0.359	0.320	0.419	1.721 ± 0.091	0.0581 ± 0.0066	2.50 ± 0.89	−0.500	–	–	–
2a	2	0–1	0.167	0.480	0.143	0.320	0.401	1.669 ± 0.036	0.0633 ± 0.0033	3.37 ± 0.55	−0.500	–	–	–
3.1a	3	0–1.5	1.166	0.304	0.223	0.320	0.385	1.626 ± 0.042	0.0691 ± 0.0047	3.46 ± 0.71	−0.500	0.227 ± 0.023	–	–
3.2a	3	1.5–1.83	2.044	4.081	–	0.320	0.385	1.626	0.0691	3.46	−0.500	0.227	0.691 ± 0.056	–
3.3a	3	1.83–2.08	2.637	7.438	–	0.320	0.385	1.626	0.0691	3.46	−0.500	0.227	0.691	1.58 ± 0.11
3a	3	0–2.08	1.578	0.599	0.456	0.301 ± 0.004	0.592 ± 0.110	1.401 ± 0.071	0.0389 ± 0.0067	2.94 ± 0.54	−0.750	–	–	–
						(b) Objective function of the type $\Phi(\mathbf{I},\boldsymbol{\theta}_{WC})$								
1b	1	0–1	2.592	–	0.146	0.360	0.365	1.574 ± 0.073	0.1016 ± 0.0169	11.08 ± 5.37	−0.500	–	–	–
2b	2	0–1	0.137	–	0.071	0.360	0.366	1.577 ± 0.018	0.0992 ± 0.0039	10.77 ± 1.22	−0.500	–	–	–
3.1b	3	0–1.5	1.167	–	0.077	0.360	0.365	1.576 ± 0.037	0.0998 ± 0.0081	8.70 ± 2.05	−0.500	0.219 ± 0.028	–	–
3.2b	3	1.5–1.83	2.787	–	–	0.360	0.365	1.576	0.0998	8.70	−0.500	0.219	0.669 ± 0.057	–
3.3b	3	1.83–2.08	4.346	–	–	0.360	0.365	1.576	0.0998	8.70	−0.500	0.219	0.669	1.50 ± 0.10
3b	3	0–2.08	1.808	–	1.489	0.325 ± 0.007	0.706 ± 0.212	1.425 ± 0.112	0.0363 ± 0.0101	2.70 ± 0.73	−0.750	–	–	–

† Label referring to the infiltration run (1, 2, or 3) and an optimization type (a or b). Note that labels beginning with 3.1, 3.2, and 3.3 refer to piecewise optimizations for a specified time period of the infiltration run.

‡ Weighted MSR is the mean weighted sum of squared residuals for cumulative infiltration $[\mathbf{I}(t,h_0)]$, TDR water contents $[\boldsymbol{\theta}_{TDR}(t)]$, and the water characteristic $[\boldsymbol{\theta}_{WC}(h)]$ components of the objective function. Weighted MSR for each component is calculated as $(1/N_i)\ \Sigma w_i \times (\text{measured} - \text{predicted})^2$, where N_i is the number of observations for the ith component and w_i is the weighting applied to the ith component.

§ Values preceded by ± are 95% confidence intervals and indicate that the parameter was fitted for a particular optimization. Parameter values without confidence intervals were fixed for the particular optimization. θ_s, saturated water contents; n, m, τ, and α are empirically fitted parameters; K_s, saturated hydraulic conductivity; and $K(h_{p1})$, $K(h_{p2})$, and $K(h_{p3})$ are the piecewise conductivity parameters.

¶ Multiply the reported numbers by this to obtain the actual numbers.

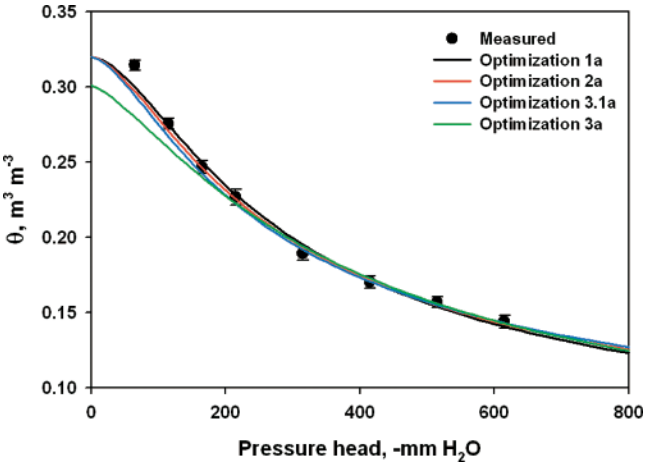

Fig. 2. Measured wetting water characteristic data and corresponding optimized solutions (Table 2). Error bars represent 95% confidence intervals for 13 extracted cores. Water characteristic data at the two largest pressure heads (−65 and −115 mm) were not included in the objective function for these optimizations. θ, volumetric water content.

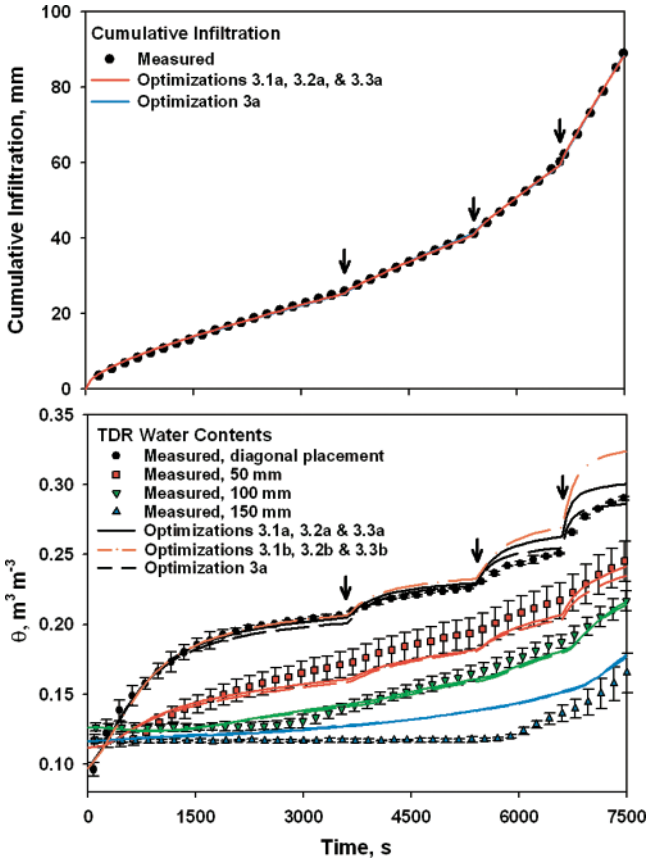

Fig. 3. Measured cumulative infiltration and water contents (θ) and the corresponding optimized piecewise (3.1a, 3.2a, and 3.3a) and van Genuchten-Mualem (VGM) (3a) solutions for Exp. 3. Predicted diagonal time-domain reflectometry water contents are also shown for optimizations 3.1b, 3.2b, and 3.3b (see Table 2). Note that the piecewise solution is not always discernible from the VGM solution. Error bars are 95% confidence limits. Arrows indicate a step change in the infiltrometer supply pressure.

mization 3a uses Eq. [2] throughout the entire range in pressure heads, the slope of $K(h)$ near saturation must be more gradual than required by 3.1a and optimizing τ yields values <-1.0. However, low values of τ led to an increased unsaturated conductivity and unrealistic drainage rates at low water contents. Durner et al. (1999) also had similar difficulties with τ converging to low values. Consequently, in optimization 3a we fixed τ to -0.75 and permitted m to vary independent of n to provide an acceptable fit of $K(h)$ throughout the entire range in pressure heads. It became apparent from optimization results across multiple h_0's (Exp. 3) that water contents measured by diagonal TDR probes were significantly lower than predicted after the initial step change in h_0 from -160 to -102 mm (Fig. 3). This difficulty may arise as a result of air entrapment occurring after the transition of the initial h_0 to a greater pressure head, whereby a portion of the air-filled pore space is isolated and prevents or delays water entry. Air entrapment would have the effect of reducing the effective pore space near saturation and generating rate dependence in soil hydraulic properties (see for example Schultze et al., 1999). We accounted for this difficulty by not including water characteristic data at pressure heads >-160 mm in the objective function and by setting θ_s to 0.32 $m^3\ m^{-3}$ instead of the fitted value obtained from the average water characteristic curve (0.364 $m^3\ m^{-3}$). Use of the above constraints to fit the three infiltration experiments (optimizations 1a, 2a, and 3.1a) resulted in a narrow range in parameter values for n, α, and K_s with overlapping 95% confidence intervals (Table 2). Optimizations 3.2a and 3.3a were obtained by sequentially fitting $K(h)$ piecewise (Eq. [4]) with the fitted parameters of 3.1a fixed. For optimization 3a, the VGM model (Eq. [2]) was fitted throughout the entire range in pressure heads, and this may have caused a divergence in the value of n to compensate for a better description of fluxes near saturation at the expense of a poorer description of the water characteristic curve (Fig. 2). The value of the cumulative weighted objective function for the piecewise optimizations ($\Phi = 3.5 \times 10^{-3}$) was marginally greater than that obtained for optimization 3a ($\Phi = 2.6 \times 10^{-3}$) where the VGM model was fitted throughout the entire range in pressure heads. Because of the high level of insensitivity of K_s and the correspondingly greater estimability of the piecewise conductivity parameters [$K(h_{p1})$, $K(h_{p2})$, and $K(h_{p3})$] exemplified by confidence limits in Table 2, use of the piecewise parameterization is recommended to reduce predictive uncertainties associated with near saturated flow.

Inverse optimizations of parameters without use of the water characteristic data of extracted cores also resulted in close fits and small standard errors. Despite the close fits to cumulative infiltration and TDR-measured water contents, these optimizations failed to correctly reproduce the measured wetting water characteristic curve (data not shown). The shape parameter n was overestimated by an average of 15% compared with optimizations 1a, 2a, and 3.1a (Table 2), leading to an underestimation of water contents in the dry region of the water characteristic. The minimum deviation between predicted and measured water contents for these optimi-

zations was positioned between $h = -165$ and -115 mm, where average predicted water contents (0.249 and 0.277 $m^3\ m^{-3}$) closely approximated average measured values from extracted soil cores (0.247 and 0.276 $m^3\ m^{-3}$). Obviously, cumulative infiltration data combined with transient water contents measured by TDR were only sufficient to predict the water content corresponding to the h_0 at which the infiltration experiment was performed. Butters and Duchateau (2002) concluded that for inverse optimizations with one-dimensional drainage in soil columns with accompanying tensiometer measurements, estimation of $K(h)$ and $\theta(h)$ at lower pressure heads required an independently measured water content at a low matric potential. In the present study, optimizations were completed that were identical to 1a, 2a, and 3.1a in Table 2 except that only a single point of the water characteristic at -615 mm H_2O was included in the objective function. These optimizations (not shown) led to estimates of n within 3% of values in Table 2 and close fits to the water characteristic curve similar to those exhibited in Fig. 2. These results suggest that the objective function should include at least a single $\theta(h)$ measurement at a pressure head significantly less than the lowest h_0 (e.g., $h_0 < -600$ mm H_2O) to help delineate the value of n and provide a better description of the water characteristic in the dry region.

Measured and predicted TDR water contents compared closely throughout the duration of the multiple supply pressure head experiment except for small deviations ($<0.03\ m^3\ m^{-3}$) exhibited by diagonally placed probes at late times and horizontally placed probes at times before the arrival of the wetting front (Fig. 3). An early predicted increase in water contents detected by the horizontal probes probably resulted from an overestimation of initial water contents between 50 and 100 mm. Overestimation of water contents for the diagonally placed probes likely resulted from the air entrapment effects discussed earlier. The time lag response of the imbibition process exhibited by TDR measured data is illustrative of experimental results and two-phase flow simulations of Schultze et al. (1999). They demonstrated that Richards' equation predicted a greater inflow and saturation percentages than two-phase flow simulations because of the loss of air continuity near saturation. This process, generally termed *dynamic nonequilibrium*, leads to $\theta(h)$ dependent on the dynamics of water flow as well as the wetting and drying history. For our optimized results, the rapid rates of predicted imbibition immediately after a change in h_0 (Fig. 3) were probably offset by a lower fitted θ_s, $K(h_0)$, and K_s. This results in an underestimated change in water content ($\partial\theta/\partial t$) at $t = 7500$ s for the diagonally placed probes and underestimated infiltration rates immediately before imposed h_0 changes. Prolonging the infiltration experiment at each h_0 might reduce these rather short-term dynamic nonequilibrium effects on optimized parameters.

Optimizations without TDR-Measured Water Contents

Optimizations were also completed with only cumulative infiltration and the water characteristic in the objective function (Table 2). All water characteristic data was included in these fits (i.e., including the observations at -65 and -115 mm H_2O). For optimizations 1b, 2b, and 3.1b (Table 2), τ was fixed at -0.5 and θ_s was estimated from a fit to the water characteristic data. The estimated value of the saturated water content ($0.360\ m^3\ m^{-3}$) is $>\theta_s$ used in optimizations 1a, 2a, and 3.1a; however, it is less than the soil porosity estimated with bulk density ($0.392\ m^3\ m^{-3}$) and there would be no justification for rejecting this value without prior knowledge of TDR-measured water contents. Optimizations without TDR-measured data resulted in close fits to cumulative infiltration and water characteristic data but with greater 95% confidence intervals for estimated parameters except for n (Table 2). Despite differences in the cumulative infiltration among the three runs, the shape parameter n was consistently fitted to a value of 1.575 ± 0.002 with m defined as $1 - (1/n)$. However, covariance estimates between K_s and α were three to 15 times greater (with positive correlation coefficients exceeding 0.998) for optimizations that did not include TDR-measured water contents. This probably resulted from the inability of the reduced data in the objective function to uniquely determine all parameters. Optimizations without TDR-measured water contents and only a single point of the water characteristic at -615 mm H_2O further exacerbated these difficulties and led to convergence problems because of large covariances between K_s and α. Predicted diagonal TDR water contents were overestimated by as much as $0.036\ m^3\ m^{-3}$ at late times for optimizations 3.1b, 3.2b, 3.3b, and 3b (Fig. 3). In contrast, predicted diagonal TDR water contents of corresponding optimizations that used TDR data (3.1a, 3.2a, 3.3a, and 3a) differed by no more than $0.022\ m^3\ m^{-3}$ from measured values. Essentially, optimizations without TDR data overestimated water contents in the surface 50 mm and predicted a steeper wetting front.

Probe Location in Reference to Wetting Front

The presence of a wetting front within the averaging volume of the TDR probe can increase measurement errors and may affect the robustness of estimated parameters when these measured water contents are used in optimizations. For the assumed axisymmetric flow field established under infiltration from a disc source, deviations from measured and predicted water contents may result from (i) physical factors that would cause a nonuniform progression of the wetting front, (ii) assuming a fixed measurement volume with uniform spatial weighting of sensitivities to permittivity, and (iii) the presence of sharp dielectric boundaries in the vicinity of the probes that would cause a dynamic dependency of spatial sensitivity (Ferré et al., 2002).

Inspection of the 95% confidence interval for TDR-measured water contents (Fig. 3) indicates that, as anticipated, diagonally placed probes were less sensitive to wetting front irregularities as compared with the horizontally placed probes. Horizontally placed probes were only partially within the wetted zone for the entire 7500 s of simulation whereas diagonally placed probes were

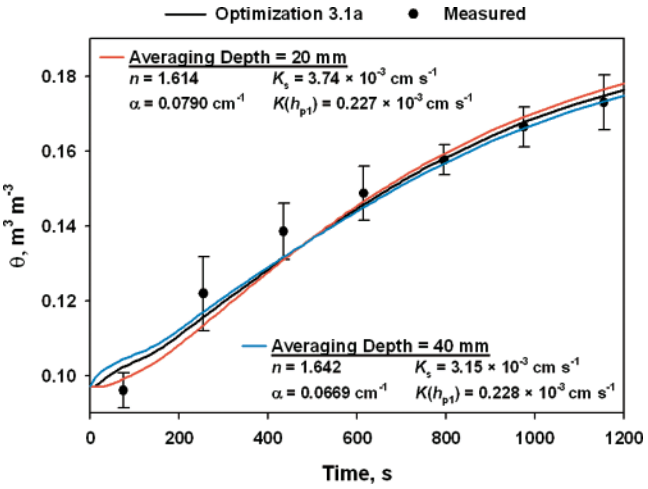

Fig. 4. Influence of assumed averaging depth on optimized parameters and predicted water contents for the diagonally placed time-domain reflectometry probe at early times. Error bars are 95% confidence intervals. θ, volumetric water content; n and α, empirically fitted parameters; K_s, saturated hydraulic conductivity; and $K(h_{p1})$, hydraulic conductivity at $h = h_{p1}$.

entirely within the wetting front by 1800 s of simulation time. In the optimized results, simulated TDR water contents were obtained by integrating nodal values of water content across an estimated probe sampling cross section of 80 mm (width) by 30 mm (depth). The influence of averaging depth on optimizations and simulated water contents (Fig. 4) show that a greater averaging depth exhibits an earlier first arrival of the wetting front. Compared with an averaging depth of 30 mm, the maximum deviation of predicted water contents with averaging depths of 20 and 40 mm was 0.006 $m^3\ m^{-3}$ and occurred at early times. However, the choice of averaging depth had a minor influence on optimized parameters because cumulative infiltration and water characteristic data were also included in the objective function.

The predicted water content distribution along the length of the center rod of a diagonally (30°) placed TDR probe and the resulting signal reflections across time are shown in Fig. 5. In contrast to other investigations involving TDR measurements in the presence of wet and dry soil boundaries (Nadler et al., 1991; Dasberg and Hopmans, 1992), the second inflection point representing the probe end was easily discernible in our signal reflections (Fig. 5) which facilitated an accurate interpretation of waveforms. Transforming to Cartesian coordinates and plotting water contents in a plane perpendicular to the TDR rods permits a better assessment of the dominant gradients in water content. In Fig. 6, a sequence of cross sections along the length of the diagonally placed TDR rods is presented for $t = 614$ s when the wetting front has just began to intrude into the averaging region. Clearly, the dominant gradients in water content (and thus dielectric permittivity) are distributed (i) along the length of the rods (x-axis) and (ii) along the z-axis transverse to the rod surface (Fig. 6). In contrast, gradients along the y-axis are subtle. Ferré et al. (2002) demonstrated that a gradient across TDR rods (along the y-axis) could introduce distortions in the interpretation of average permittivity and errors in the determination of the water contents. In contrast, Ferré et al. (2002) show water content gradients along the z-axis during the advance of a wetting front generated only small differences in water contents between simulated point values and those that would be measured with a trifilar probe on the basis of the dielectric permittivity distribution. Additionally, inverse optimization with these TDR-measured water contents permitted the recovery of hydraulic parameters in close agreement with known values. Because variations in permittivity tend to be independent of the x-axis (Knight, 1992) and because the apparent permittivity can be approximated as an arithmetic average of true permittivities distributed in a narrowly defined region along the z-axis, we expect that the averaging of water contents across the three-dimensional sampling volume results in an accurate estimation of water contents for these diagonally placed trifilar probes. Obviously, these interpretations are geometry dependent as exemplified by considering that larger gradients in water content would be generated along the y-axis by use of an infiltrometer base with a smaller diameter in conjunction with the same TDR probes.

CONCLUSIONS

Inverse optimizations with measured cumulative infiltration and transient water contents from diagonally placed TDR probes provided an efficient method for estimation of hydraulic properties. The use of diagonal TDR-measured water contents in the objective function improved the predicted redistribution of soil water and decreased covariances between parameter pairs that led to better parameter estimability. Besides infiltration and TDR-measured water contents, the objective function should also include at least one independent measurement of $\theta(h)$ at a pressure head sufficiently less than the lowest h_0 to provide a better description of the water characteristic in the dry region. A time lag in measured water contents compared with estimated water contents for the diagonally placed probes immediately after step changes in supply pressure likely resulted from the loss of air phase continuity near saturation. Despite this difficulty, optimized simulations were able to predict water contents across a three-dimensional region within 0.03 $m^3\ m^{-3}$ of values measured by horizontal TDR probes buried at several depths below the surface.

The use of 150-mm TDR probes inserted diagonally (30°) into the soil surface permitted the sampling of water contents within the wetted perimeter shortly after initiation of infiltration. Use of a different averaging depth for these probes to calculate water contents for optimizations caused only small deviations in predicted water contents that were less than the observed experimental error for replicated infiltration experiments. For these diagonally placed probes, the dominant gradients in water content were in directions that minimized errors associated with assuming a uniform weighting of water content within the sampling volume.

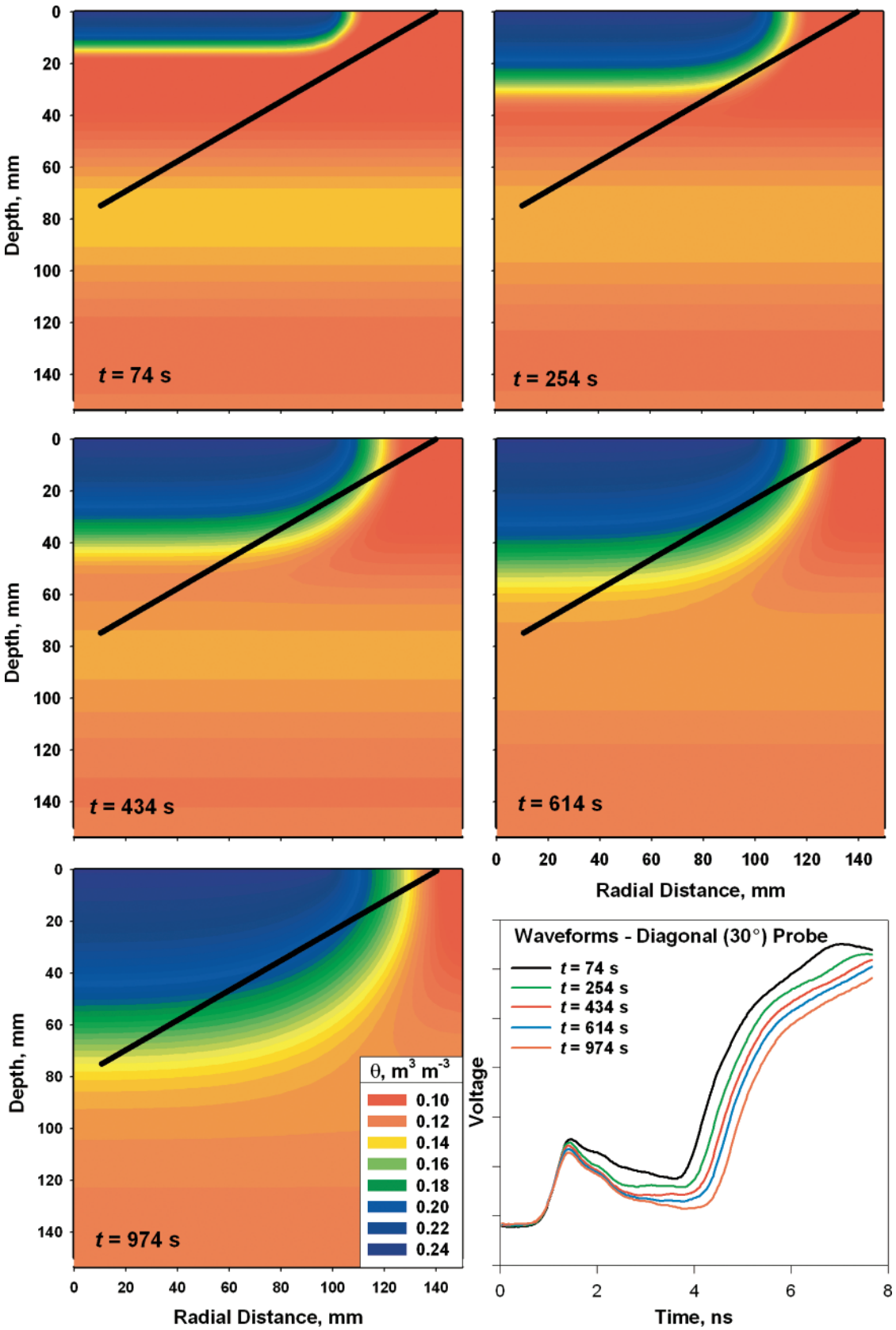

Fig. 5. Two-dimensional progression of wetting front (Optimization 3.1a) and corresponding time-domain reflectometry waveforms for a diagonally (30°) placed probe. The diagonal line represents the center rod of a trifilar probe.

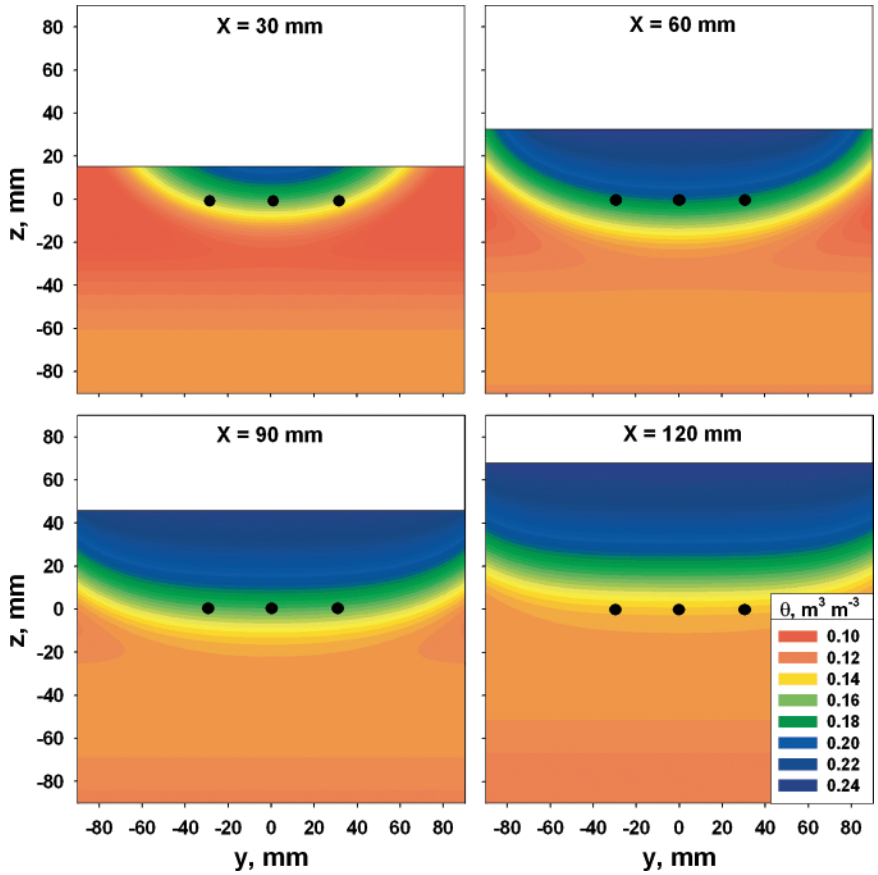

Fig. 6. Simulated cross section of water contents (θ) at t = 614 s (Optimization 3.1a) in Cartesian coordinates at several positions along the x-axis that runs parallel with the time-domain reflectometry (TDR) rods. The filled circles represent the positions of the TDR probes and the border between the white and filled regions represents the soil surface boundary.

ACKNOWLEDGMENTS

The authors gratefully acknowledge the anonymous reviewers for their helpful comments and suggestions.

REFERENCES

Butters, G.L., and P. Duchateau. 2002. Continuous flow method for rapid measurement of soil hydraulic properties. I. Experimental considerations. Available at www.vadosezonejournal.org. Vadose Zone J. 1:239–251.

Dasberg, S., and J.W. Hopmans. 1992. Time domain reflectometry calibration for uniformly and nonuniformly wetted sandy and clayey loam soils. Soil Sci. Soc. Am. J. 56:1341–1345.

Durner, W., E. Priesack, H.-J. Vögel, and T. Zurmühl. 1999. Determination of parameters for flexible hydraulic functions by inverse modeling. p. 817–829. *In* M.Th. van Genuchten et al. (ed.) Proc. Int. Workshop Characterization and Measurement of the Hydraulic Properties of Unsaturated Porous Media, Riverside, CA. 22–24 Oct. 1997. Univ. of California, Riverside.

Evett, S.R. 1998. Coaxial multiplexer for time domain reflectometry measurement of soil water content and bulk electrical conductivity. Trans. ASAE 41:361–369.

Evett, S.R. 2000a. The TACQ program for automatic time domain reflectometry measurements: I. Design and operating characteristics. Trans. ASAE 43:1939–1946.

Evett, S.R. 2000b. The TACQ program for automatic time domain reflectometry measurements. II. Waveform interpretation methods. Trans. ASAE 43:1947–1956.

Ferré, P.A., J.H. Knight, D.L. Rudolph, and R.G. Kachanoski. 1998. The sample areas of conventional and alternative time domain reflectometry probes. Water Resour. Res. 34:2971–2979.

Ferré, P.A., H.H. Nissen, and J. Šimůnek. 2002. The effect of the spatial sensitivity of TDR on inferring soil hydraulic properties from water content measurements made during the advance of a wetting front. Available at www.vadosezonejournal.org. Vadose Zone J. 1:281–288.

Kachanoski, R.G., I.J. Van Wesenbeeck, P. Von Bertoldi, A. Ward, and C. Hamlen. 1990. Measurement of soil water content during three-dimensional axial-symmetric water flow. Soil Sci. Soc. Am. J. 54:645–649.

Knight, J.H. 1992. Sensitivity of time domain reflectometry measurements to lateral variations in soil water content. Water Resour. Res. 28:2345–2352.

Knight, J.H., I. White, and S.J. Zegelin. 1994. Sampling volume of TDR probes used for water content monitoring. Symp. on Time Domain Reflectometry in Environmental, Infrastructure and Mining Applications, Evanston, IL. 7–9 Sept. 1994. U.S. Bureau of Mines, Evanston, IL.

Nadler, A., S. Dasberg, and I. Lapid. 1991. Time domain reflectometry measurements of water content and electrical conductivity of layered soil columns. Soil Sci. Soc. Am. J. 55:938–943.

Schultze, B., O. Ippisch, B. Huwe, and W. Durner. 1999. Dynamic nonequilibrium during unsaturated water flow. p. 877–892. *In* M.Th. van Genuchten et al. (ed.) Proc. Int. Workshop, Characterization and Measurement of the Hydraulic Properties of Unsaturated Porous Media, Riverside, CA. 22–24 Oct. 1997. Univ. of California, Riverside.

Schwartz, R.C. 2002. The IDSfit code for inverse estimation of field hydraulic properties using a disc infiltrometer. Conservation and Production Research Lab., USDA-ARS, Bushland, TX.

Schwartz, R.C., and S.R. Evett. 2002. Estimating hydraulic properties of a fine-textured soil using a disc infiltrometer. Soil Sci. Soc. Am. J. 66:1409–1423.

Šimůnek, J., and M.Th. van Genuchten. 1996. Estimating unsaturated soil hydraulic properties from tension disc infiltrometer data by numerical inversion. Water Resour. Res. 32:2683–2696.

Šimůnek, J., and M.Th. van Genuchten. 1997. Estimating unsaturated soil hydraulic properties from multiple tension disc infiltrometer data. Soil Sci. 162:383–398.

Topp, G.C., J.L. Davis, and A.P. Annan. 1980. Electromagnetic determination of soil water content: Measurements in coaxial transmission lines. Water Resour. Res. 16:574–582.

van Genuchten, M.Th. 1980. A closed-form equation for predicting the hydraulic conductivity of unsaturated soils. Soil Sci. Soc. Am. J. 44:892–898.

van Genuchten, M.Th., and D.R. Nielsen. 1985. On describing and predicting the hydraulic properties of unsaturated soils. Ann. Geophys. 3:615–628.

Wang, D., S.R. Yates, and F.F. Ernst. 1998. Determining soil hydraulic properties using tensions infiltrometers, time domain reflectometry, and tensiometers. Soil Sci. Soc. Am. J. 62:318–325.

Warrick, A. 1992. Models for disc infiltrometers. Water Resour. Res. 28:1319–1327.